Int. J. Electrochem. Sci., 6 **(2011)** 206 - 221

International Journal of
ELECTROCHEMICAL
SCIENCE
www.electrochemsci.org

Synthesis and Properties of Polyaniline/ferrites Nanocomposites

A. H. Elsayed[1], *M. S. Mohy Eldin*[2,*], *A.M.Elsyed*[2], *A. H. Abo Elazm, E.M.Younes*[3] *and H. A. Motaweh*[3]

[1] Physics Department, Faculty of Science, Alexandria University, Egypt,
[2]Advanced Technology and New Material Research Institute, Mubarak City for Scientific Research and Technological Applications, New Boarg El-Arab City 21934, Alexandria, Egypt,
[3]Physics Department, Faculty of Science, Alexandria University, Damanhour Branch, Egypt
[*]E-mail: mohyeldinmohamed@yahoo.com

Received: 21 October 2010 / *Accepted:* 30 October 2010 / *Published:* 1 January 2011

Polyaniline (PANI-EB) containing MFe_2O_4 (M is an element in a divalent state; M^{2+} = Fe^{2+}, Co^{2+}, Ni^{2+}, Mn^{2+}, and Zn^{2+}) were prepared by chemical method. The results of this investigation indicate that; i) the size of MFe_2O_4 in PANI is in the range 10 to 20 nm. ii) the MFe_2O_4 nanoparticles have the characteristic reflections of the Fd-3m spinel cubic structure. iii) the presence of ferromagnetic phase in PANI/Fe_3O_4 and PANI/$CoFe_2O_4$ samples, while samples containing Ni^{2+}, Mn^{2+}, and Zn^{2+} showed a superparamagnetic behavior. The results of Thermogravimetric analysis indicated that the addition of MFe_2O_4 nanoparticles to PANI improved the nanocomposites thermal stability. The interaction between MFe_2O_4 nanoparticles and PANI matrix may be occurred by the formation of the hydrogen bonding between the amine group of PANI and Oxygen of MFe_2O_4.

Keywords: Polyaniline, nanocomposites, magnetic properties, ferrite, conducting polymers, thermal stability.

1. INTRODUCTION

Organic–inorganic nanocomposites with an organized structure has been extensively studied because they combine the advantages of the inorganic materials (mechanical strength, electrical and magnetic properties and thermal stability) and the organic polymers (Flexibility, dielectric, ductility and processibility), which are difficult to obtain from individual components [1- 4].

Among conducting polymers, polyaniline (PANI) is probably the most widely studied due to its several unique properties [5, 6]. It ease of preparation, light weight, low cost, better electronic, optical properties, highly stable in air and soluble in various solvents, and good processibility [7-9]. On the other hand it can be used in many applications, such as electromagnetic interference (EMI) shielding,

electro-catalysts, rechargeable battery, light-emitting diodes (LEDs), chemical sensor, biosensor, corrosion devices and microwave absorption [10, 11]. PANI exhibits dramatic changes in its electronic structure and physical properties at protonated state. Depending on the oxidation level, PANI can be synthesized in various insulating forms such as the fully reduced leucoemeraldine base (LEB), half-oxidized emeraldine base (PANI-EB) and fully oxidized pernigraniline base (PNB). Of these three forms, PANI-EB is the most stable and widely investigated polymer in this family. PANI-EB differs substantially from LEB and PNB in the sense that its conductivity can be tuned via doping from 10^{-10} up to 100 S/cm and more, whereas the LEB and PNB form cannot be conducting [9]. The conducting emeraldine salt form (PANI-ES) is achieved by doping with aqueous protonic or functionalized acids where protons are added to the –N= sites. This leads to an increase in the conductivity by more than ten orders of magnitude depending on the strength of the acid and the method of processing [12]. PANI composites with magnetic and conducting properties have been studied by Wan's group [13]. They prepared materials with very low coercive force (H_c ~ 0) and relatively high saturation magnetization (M_s~ 72 emu/g). The soft magnetic spinel ferrites of the form $A^{2+}B^{3+}{}_2O_4$ such as Fe_3O_4, $CoFe_2O_4$, $NiFe_2O_4$, $MnFe_2O_4$, and $ZnFe_2O_4$ have widely used in microwave devices due to their high saturation magnetization, high permeability, high electrical resistivity and low eddy current losses [13-15].

In this article, PANI-EB was selected as standard materials because it was prepared at alkaline condition and suitable for the addition of magnetic nanoparticles. We have synthesis the nanocomposites of PANI/MFe_2O_4 by in situ precipitation method [9, 12, and 16]. The structure, surface morphology and thermal stability of free PANI and PANI/MFe_2O_4 nanocomposites have been studied.

2. EXPERIMENTAL

2.1. Materials

PANI-EB and PANI/MFe_2O_4 composite powders were prepared according to the previously reported method [16-18]. Aniline monomer was distilled under reduced pressure and stored below 0 C°, Hydrochloric acid (HCl), Ammonium peroxydisulfate (APS), NaOH, $FeCl_3{\cdot}6H_2O$ and $FeCl_2{\cdot}6H_2O$, $CoCl_2{\cdot}6H_2O$, $NiCl_2{\cdot}6H_2O$, $MnCl_2{\cdot}6H_2O$, $ZnCl_2{\cdot}6H_2O$, distilled water, acetone 99 %, ammonium hydroxide 37 % and methanol 99% were used without further purification.

2.1.1. Preparation of polyaniline (PANI-EB):

PANI was synthesized via an in-situ oxidative polymerization, in which aniline and ammonium peroxysulfate (APS) were used as monomer and initiator, respectively. Initially, aniline was dispersed in 1 M HCl by vigorous stirring. APS (0.55 mol) was dissolved in 1 M HCl and dropped into the reactor for 4 h. After dropping the initiator, the mixture was kept constant stirring and the solution is placed inside an ice bath maintaining stirring for another 24 h. When the reaction was finished, the

dark green precipitate resulting from the polymerization reaction was filtered and washed with distilled water, acetone, and methanol sequentially in order to remove the excess initiator, monomer, and oligomer. This precipitate is then dried in an oven at 40Cº for 24h.

For deprotonation, PANI was suspended in excess of 1 M ammonium hydroxide for several hours, until pH reached 9. The resulting polymer bases were separated on a filter and washed with distilled water, acetone, and methanol until the filtrate becomes transparent. This precipitate is then dried in an oven at 40Cº for 24h.

2.1.2. Preparation of PANI /MFe_2O_4 nanocomposites:

PANI/MFe_2O_4 nanocomposites were prepared according to the method previously described [9, 12, and 16]. MFe_2O_4 nanoparticles were grown ‘‘in situ’’ with the PANI.

A mixed solution of MCl_2 (1.0M) and $FeCl_3.6H_2O$ (1.5M) as oxidant were dissolved in water with vigorous stirring at room temperature. A specific volume of aniline was added to the above mixed solution. After 4 h of reaction, the solution of NaOH was added. The pH value was controlled during the entire experiment to pH=11. A black precipitant of PANI was observed after 10 h. The resulting polymer nanocomposite was poured into water and filtered. Each wash step was carried out until the filtrate became clear and colorless. Finally, the polymer composite was washed with distilled water, methanol and acetone, then dried overnight in a vacuum oven at 40 Cº.

2.2. Characterization

The XRD patterns of the polyaniline nanocomposites were recorded using a Schimadszu, 7000, USA diffractometer with Cu Kα radiation (λ = 0.15418 nm). The corresponding intensities were measured for 2θ angles ranging from 10° to 80° with a step 0.07° per second. The morphology of the particles and their agglomerates was studied using scanning electron microscopy (SEM) type JEOL JSM 6360LA, Japan microscope. Size measurements of polyaniline nanocomposites were studied by PSA using a Beckman Coulter N5 Submicron particle size analyzer. Infrared spectra of samples were recorded on a Shimadzu, FTIR 8400s, Japan spectrometer in the range of 400–4000 cm^{-1}. Thermal stability of samples were also studied by TGA using Shimadzu, TGA 50, Japan Thermogravimetric with heating rate of 10 C°/min and flow air rate at 20 ml/min in the temperature range from 25 to 900 C°. Magnetic hysteresis loops were recorded at room temperature using a vibrating sample magnetometer (VSM) (9600-1-vsm, LDJ, U.S.A.) with a maximum magnetic field of 10 kOe.

3. RESULTS AND DISCUSSION

3.1. Chemical analysis

Table 1 shows the percentage of MFe_2O_4 nanoparticles in PANI/MFe_2O_4 nanocomposites measured by chemical analysis, which indicates the presence of greater amount of ferrite than PANI in the nanocomposites.

Table 1. The ratio between PANI and MFe_2O_4 nanocrystals in PANI/MFe_2O_4 nanocomposites:

Samples	PANI wt%	MFe_2O_4 wt%
PANI/Fe_3O_4	28.88	71.12
PANI/ $CoFe_2O_4$	31.21	68.79
PANI/ $NiFe_2O_4$	45.97	54.03
PANI /$MnFe_2O_4$	48.13	51.87
PANI /$ZnFe_2O_4$	43.47	56.53

3.2. X-ray diffraction analysis (XRD)

Fig. 1. shows the XRD spectra of all synthetic PANI/MFe_2O_4 nanocomposites. The related data are given in Table 2. The XRD spectrum for free PANI (Fig.1.a) does not show any sharp peaks suggesting an amorphous nature of PANI. However, the polymer displays a diffuse broad peak ranging from 15° to 30°, which is consistent with the results obtained by other research groups [4, 19, and 20]. The PANI/MFe_2O_4 nanocomposites (Fig. 1. b-f) show crystalline peaks due to the presence of ferrite in these nanocomposites. The main broad peak of the PANI disappeared because the MFe_2O_4 nanoparticles interfered with PANI chains.

Table 2. Comparison of XRD data of PANI/MFe_2O_4 nanocomposites with the previously published data.

PANI/Fe_3O_4			**PANI/ $CoFe_2O_4$**		**PANI/ $NiFe_2O_4$**		**PANI /$MnFe_2O_4$**		**PANI /$ZnFe_2O_4$**		**(hkl) of MFe_2O_4**
2θ(°)	d(Å)	d(Å) Ref[a]	d(Å)	d(Å) ref [b]	d(Å)	d(Å) ref [c]	d(Å)	d(Å) ref [d]	d(Å)	d(Å) ref [e]	
18.37	4.82	4.85	4.85	4.89	4.79	4.82			4.82	4.85	111
22.27	3.99	___	3.51	___	3.61	___	3.93	___	3.51	___	____
30.18	2.96	2.97	2.96	2.95	2.84	2.95	2.99	3.02	2.97	2.99	220
35.59	2.51	2.53	2.52	2.51	2.54	2.51	2.56	2.58	2.55	2.54	311
43.27	2.09	2.1	2.09	2.08	2.10	2.08	2.15	2.13	2.10	2.10	400
57.19	1.60	1.61	1.61	1.61	1.60	1.60	1.60	1.64	1.61	1.62	511
62.83	1.48	1.48	1.48	1.48	1.47	1.48	1.52	1.54	1.50	1.49	440

[a](Card No. PDF 00-001-1111). [b](Card No. PDF 00-001-1121).
[c](Card No. PDF 00-003-0875). [d](Card No. PDF 00-002-1392).
[e](Card No. PDF 00-001-1108).

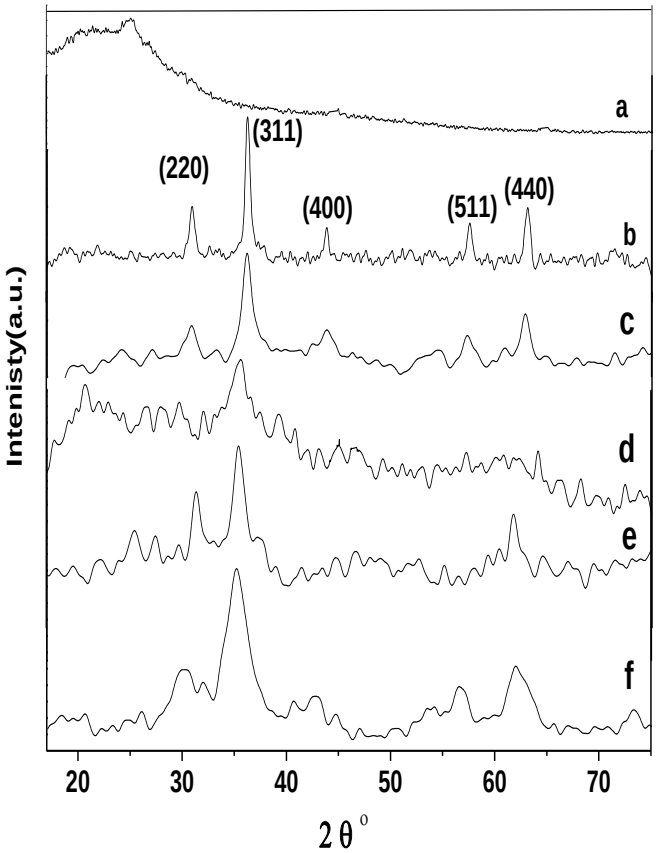

Figure 1. Comparison of XRD patterns of (a) free PANI, (b) PANI/Fe_3O_4, (c) PANI/ $CoFe_2O_4$, (d) PANI/ $NiFe_2O_4$, (e) PANI /$MnFe_2O_4$, (f) PANI /$ZnFe_2O_4$.

According to the reflection peaks in Fig. 1, the XRD pattern of PANI/MFe_2O_4 nanocomposites Fig (1), showed that the main characteristic peaks of MFe_2O_4 are near 30.18, 35.59, 43.27, 57.19, 62.83 (2θ) and with indexed to (220), (311), (400), (511), and (440) planes respectively. These are consistence with the characteristic reflections of the Fd-3m spinel cubic structure [20-22].

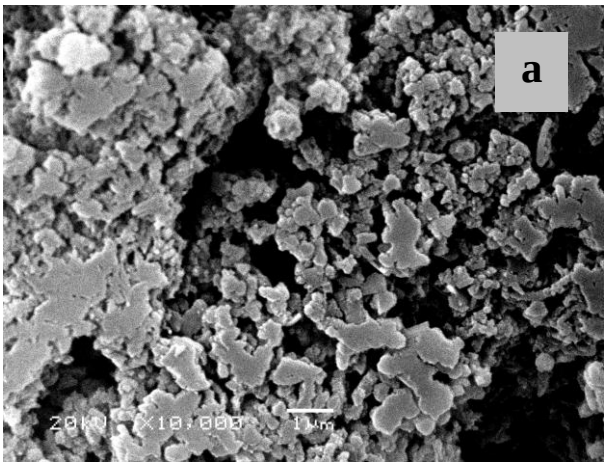

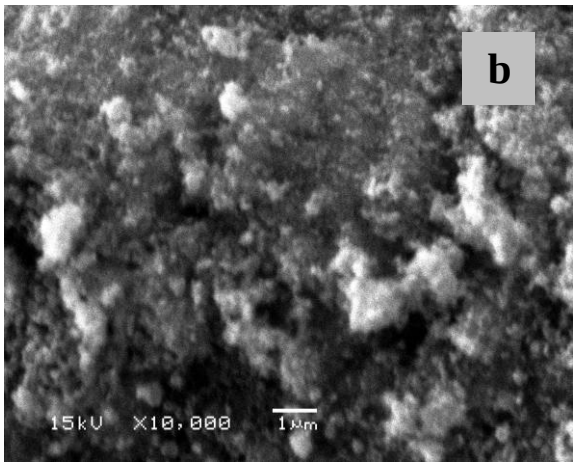

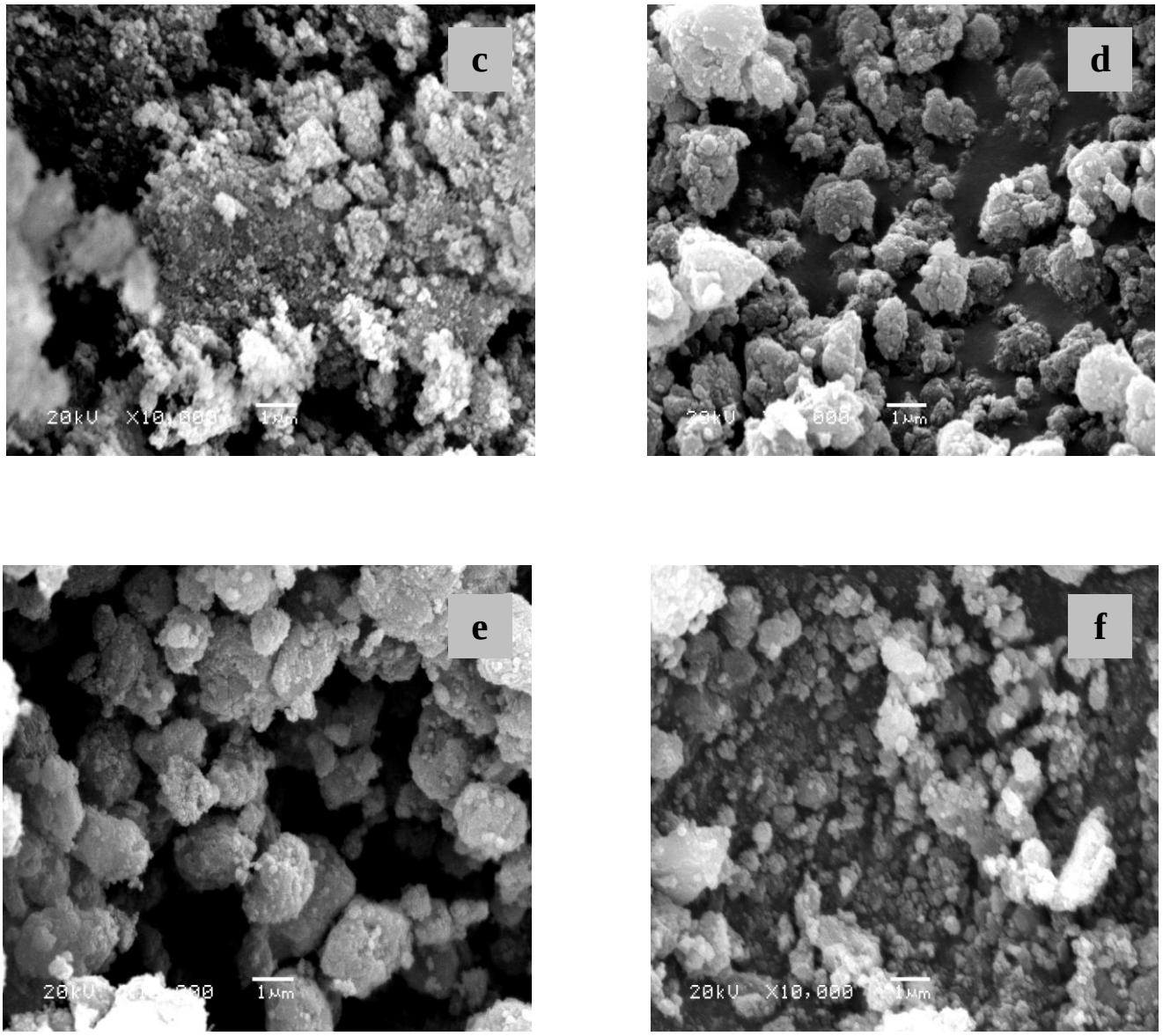

Figure 2. Comparison between SEM images of PANI/MFe_2O_4 nanocomposites at the same scales (a) pure PANI, (b) PANI/Fe_3O_4, (c) PANI/$CoFe_2O_4$, (d) PANI/$NiFe_2O_4$, (e) PANI/$MnFe_2O_4$, and (f) PANI/$ZnFe_2O_4$.

The average grain size of MFe_2O_4 nanoparticles in PANI/MFe_2O_4 nanocomposites have been calculated from the line broadening using the Debye –Scherrer formula given by:

$$D = k\lambda/\beta\cos\theta \qquad (1)$$

where D is the average crystallite size (in Å), k is the shape factor which is often assigned a value of 0.89, λ is the wavelength of Cu Kα radiation (1.5418 Å), β is the full width at half maximum of the diffraction peaks taking in to consideration the correction due to instrumental broadening (0.09°)

and θ is the Bragg's angle [12, 23]. The values of β and particle size D were calculated and are listed in Table 3.

The calculated particle size D using the Scherrer formula are differ from peak to another peak , which may be due to the strain effect on the line width [24].

Table 3. The calculated values of D and β for MFe_2O_4 nanoparticles in PANI/MFe_2O_4 nanocomposites for all peaks at different planes.

hkl	PANI/Fe_3O_4		PANI/ $CoFe_2O_4$		PANI/ $NiFe_2O_4$		PANI /$MnFe_2O_4$		PANI/ $ZnFe_2O_4$	
	β(rad) $*10^{-2}$	D(nm)	β (rad) $*10^{-2}$	D(nm)	β (rad) $*10^{-2}$	D(nm)	β (rad) $*10^{-2}$	D(nm)	β (rad) $*10^{-2}$	D(nm)
220	1.11	12.97	0.96	14.93	0.81	17.64	1.07	13.46	1.26	11.39
311	1.05	13.80	1.25	11.64	1.43	10.02	1.28	11.35	1.32	10.86
400	0.90	16.60	1.19	12.46	0.90	16.82	1.32	11.30	1.16	12.79
511	0.99	15.98	1.10	14.33	0.85	18.61	0.92	17.43	0.88	18.02
440	1.09	14.83	1.01	16.02	0.93	17.67	0.96	16.75	1.26	12.82

The values of the grain size D of PANI/MFe_2O_4 samples were estimated over the range 11 to 18 nm and are listed in Table 3.

Lattice parameter (*a*) was calculated for the cubic structure and was found to be 8.32Å, 8.36Å, 8.42 Å, 8.49 Å, and 8.46 Å for Fe_3O_4, $CoFe_2O_4$, $NiFe_2O_4$, $MnFe_2O_4$ and $ZnFe_2O_4$ nanoparticles respectively. These values are in good agreement with other published data [15, 25].

3.3. SEM for powder

The surface morphology and particle sizes of PANI/MFe_2O_4 nanocomposites were determined using SEM. Fig. 2. shows a comparison between SEM images of PANI/MFe_2O_4 nanocomposites and the free PANI. The results are in agreement with references [12, 17, 26, and 27]. Fig. 2.a. represents the SEM image of PANI-EB powder. This sample was prepared in absence of acid. It exhibits a porous and irregular structure of the low conductive surface. There are a large number of clews whose diameter is about 29 nm. Figs (2. b-f) correspond to the SEM images of the PANI/MFe_2O_4 magnetic nanocomposites. The irregular shapes and the porous nature of the compacted powders are evidenced by the images taken at high magnification. These figures indicate that, the surface of these nanocomposites was rough and the nanocomposites exhibit, more or less, spherical morphology. Also, the diameter of the individual nanoparticle in PANI/MFe_2O_4 nanocomposites was ranging from 10 to 40 nm. It is clear from Fig. 2. that the PANI can minimize the aggregation of nanoparticles due to the repulsive forces between magnetic nanoparticles and PANI. It is concluded from SEM images, that the

average size of the particles of Fe_3O_4, $CoFe_2O_4$, $NiFe_2O_4$, $MnFe_2O_4$ and $ZnFe_2O_4$ in nanocomposites is 30, 22, 17, 21 and 22 nm respectively.

3.4. Particle Size Analyzer (PSA)

Table 4. shows the particle size of the PANI/MFe_2O_4 nanocomposites as determined by PSA in aqueous solution. Size distribution of these nanocomposites is in the range from 10 nm to 100 nm.

It can be seen from Table 4 that the size measurements using PSA method is larger than the other two methods (XRD and SEM). This is because XRD spectra and SEM image measured only the size of MFe_2O_4 nanoparticles exist in the polymer in the dry state.

Table 4. Comparison between the sizes measured of samples by XRD, SEM and PSA for PANI/MFe_2O_4 nanocomposites.

Samples	Mean size of samples (nm)		
	XRD (311)	SEM	PSA
PANI/Fe_3O_4	13.8	30	34.8
PANI/ $CoFe_2O_4$	11.6	22	24.3
PANI/ $NiFe_2O_4$	10	17	25.7
PANI /$MnFe_2O_4$	11.3	21	36.8
PANI /$ZnFe_2O_4$	10.9	22.1	34.1

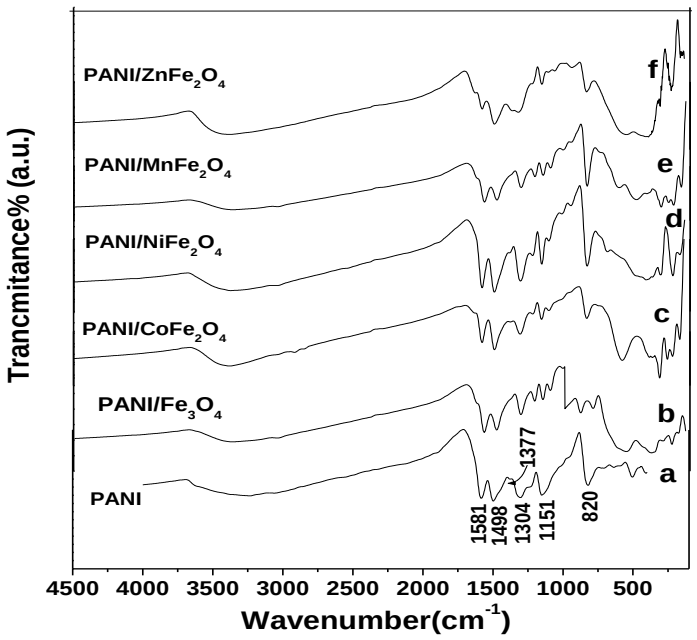

Figure 3. FTIR spectra of PANI and PANI/MFe_2O_4 nanocomposites.

3.5. FTIR spectra

Fig.3. Shows the FTIR characteristic peaks of pure PANI, and PANI/MFe_2O_4. nanocomposites. Table 5, summarized the main wavenumber and assignments of the detected active IR-bands. It shows also the comparison between the observed absorption bands of free PANI and the observed absorption bands of PANI/MFe_2O_4 nanocomposites.

Table 5. Comparison between the observed absorption bands of free PANI and PANI/MFe_2O_4 nanocomposites.

Free PANI cm^{-1}	PANI/ Fe_3O_4 cm^{-1}	PANI/ $CoFe_2O_4$ cm^{-1}	PANI/ $NiFe_2O_4$ cm^{-1}	PANI/ $MnFe_2O_4$ cm^{-1}	PANI/ $ZnFe_2O_4$ cm^{-1}	Vibrational assignments
1581	1577	1583	1585	1578	1583	Benzenic-quinonic nitrogen
1498	1488	1495	1499	1487	1495	C-C aromatic
1377	1315	1383	1389	1315	1367	Aromatic amine
1303	1217	1311	1311	1217	1325	-N =quinoid=N-
1151	1158	1159	1159	1157	1157	C-N-C
820	800	837	835	843	837	C-H out-of-plane
___	563	582	690	615	552	Tetrahedral sites
___	409	411	417	492	410	octahedral sites

Fig 3.a shows the FTIR spectra of free PANI-EB. The vibrational bands observed for polyaniline are reasonably explained on the basis of the normal modes of polyaniline. The characteristic bands in the IR spectra of free PANI occur at 1581, 1498, 1377, 1304, 1151 and 820 cm^{-1} in agreement with the observed bands shown in references [4, 28, and 29]. The band at 3236-3840 cm^{-1} is assigned to the NH stretching vibration of the $–C_6H_4NHC_6H_4–$ group. The one at 3063 cm^{-1} is assigned to the vibration associated with the NH_2^+ part in the

$–C_6H_4\ NH_2^+C_6H_4–$ group. The bands at 1581 cm^{-1} and 1498 cm^{-1} are attributed to the C=N and C=C stretching modes of vibration for the quinonoid and benzenoid units of the polymer, 1304 cm^{-1} attributed to the C–N stretching of secondary aromatic amine (-N-benzenoid-N-), while the bands at 1377 cm^{-1} and 1151 cm^{-1} are assigned to the C–N stretching mode of benzenoid units (in-plane-bending modes). The bands at 1151 cm^{-1} were explained as an electronic band or the vibrational band of nitrogen quinone (C=N stretching -N =quinoid=N-). The peak at 820 cm^{-1} is attributed to C–C and

C–H for the benzenoid unit and arises from aromatic CH out-of-plane bending in the 1,4-disubstituted benzene ring which has been used as a key to identifying the type of substituted benzene.

The IR absorption bands of solids in the range 100 – 1000 cm^{-1} are usually assigned to vibrations of ions in the crystal lattice. In ferrites, the metal ions are usually situated in two different sublattices, designated as tetrahedral and octahedral sites according to the geometrical configuration of the oxygen nearest neighbors. The vibrational spectra of spinel ferrites (MFe_2O_4) are attributed the high-frequency band (600–580 cm^{-1}) to the intrinsic vibration of the tetrahedral sites and the low-frequency band (440–400 cm^{-1}) to the octahedral sites [19, 29].

The spectrum of these nanocomposites is compared with that of the free PANI shown in Fig. (3. a.). Important differences in peak positions suggest that some reactions take place on the surface of nanoparticles. For PANI/Fe_3O_4 (Fig 3.b.) nanocomposites the bands at 800 and 887 cm^{-1} are due to iron oxide lattice deformations and to OH groups bound to the surface of Fe_3O_4 nanoparticles, but the peak appeared at 563 cm^{-1} in the nanocomposite is due to Fe–O stretching band of Fe_3O_4 [30 - 34].

Fig. (3. b-f) together with Table 5 show that the absorption bands at 563, 582, 690, 615, and 552 cm^{-1} are intrinsic vibrations of the tetrahedral sites, while the absorption bands at 409, 411, 417, 492, and 410 cm^{-1} are intrinsic vibrations of the octahedral sites for Fe_3O_4, $CoFe_2O_4$, $NiFe_2O_4$, $MnFe_2O_4$, $ZnFe_2O_4$ nanoparticles embedding in PANI matrix respectively [35, 36]. All other bands of these nanocomposites correspond to vibration modes in the polyaniline matrix with little shifts compared with pure PANI. This may indicate that PANI is formed together with the ferrites nanocrystal. The incorporation of MFe_2O_4 nanoparticles with PANI lead to shift some FTIR bands of the PANI in the nanocomposites. The results reveal that there exists an interaction between ferrite and PANI chains, and suggests the effective formation of the PANI/MFe_2O_4 nanocomposites.

3.6. TGA measurements

The TGA measurements of PANI/MFe_2O_4 nanocomposites show that MFe_2O_4 nanoparticles may improve the thermal stability of these nanocomposites. The TGA was performed under nitrogen atmosphere to minimize undesired mass increase due to the oxidation reactions in the ferrite, and PANI be thermally decomposed almost completely [23]. Fig. 4. shows the TGA curves of PANI/MFe_2O_4 nanocomposites compared with free PANI. TGA curve of free PANI show that around 96 % in weight was lost when the sample was heated from room-temperature up to 736 C°. The decomposition temperatures obtained from thermograms of pure PANI exhibits two stage weight-loss behavior. The first step at 38 to 117 C° which is due to expulsion of water molecules, the evaporation of residual solvents such as methanol, acid and small molecules from polymer structure. The weight loses during this stage is about 11.67%. The second step at 263 -736 C° shows decomposition or thermal degradation of the polymer, and has the great weight loss of about 84.58% [9, 23, and 37].

The decomposition temperatures obtained from thermograms of PANI/MFe_2O_4 nanocomposites exhibit two stage weight-loss behavior. The first step is due to expulsion of water molecules, the evaporation of residual solvents such as methanol from polymer matrix, while the second step is a decomposition step. The two stage weight loss of these nanocomposites are listed in

Table 6 together with the pure PANI. The weight loss of all samples which heated from room-temperature up to 736 C° is also presented. The weight loss at all stage is much less for nanocomposites compared to that of pure PANI. The result of PANI/Fe_3O_4 nanocomposite is in agreement with that recorded in literature [9, 23]. The difference between PANI/MFe_2O_4 nanocomposites in weight loss Table 6 may be due to the difference in their chemical and geometrical nature.

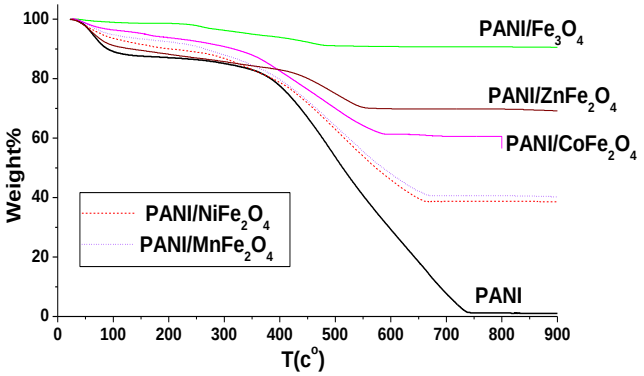

Figure 4. The TGA curves of PANI and PANI/MFe_2O_4 nanocomposites.

Fig.4. and Table 6 show that the thermal stability of the PANI/MFe_2O_4 nanocomposites is higher than that of pure PANI. This may be due to the interaction between MFe_2O_4 nanoparticles and PANI chain.

Table 6. The weight loss % at different decomposition temperature steps for PANI and PANI/MFe_2O_4 nanocomposites.

Samples	Weight loss% first step	Weight loss% second step	Weight loss% Room Temp up to 736 C°
PANI	11.67	84.58	96.25
PANI/Fe_3O_4	1.15	7.29	8.44
PANI/$CoFe_2O_4$	5.40	33.01	38.41
PANI/$NiFe_2O_4$	7.92	52.82	60.74
PANI/$MnFe_2O_4$	5.30	53.36	58.66
PANI/$ZnFe_2O_4$	8.82	20.85	29.67

3.7. Magnetic properties

Magnetization measurements of PANI/MFe_2O_4 nanocomposites were carried out using a vibrating sample magnetometer (VSM) at room temperature.

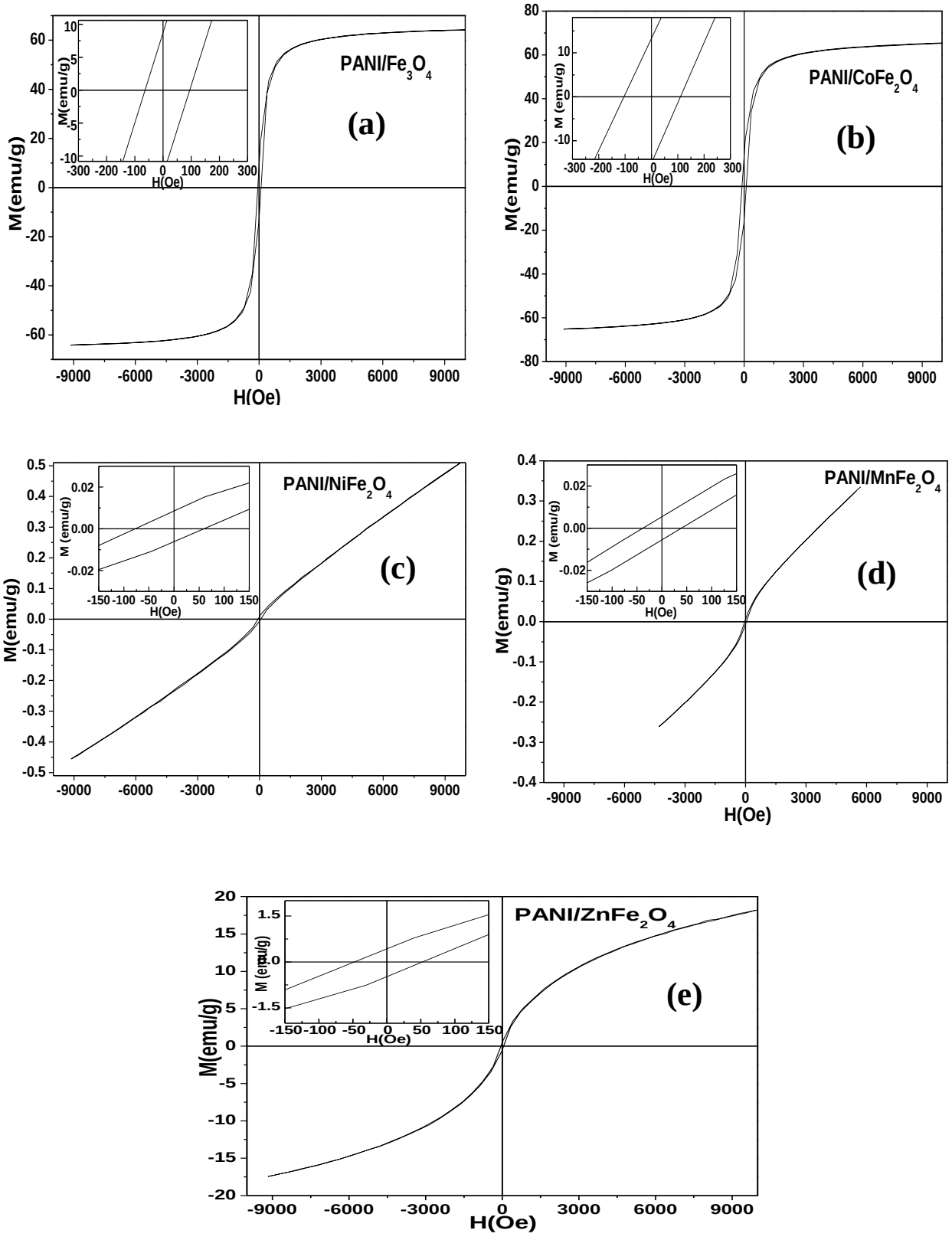

Figure 5. Magnetic hysteresis loops for PANI/MFe_2O_4 nanocomposites at room temperature. Inset: low field magnetization curves at room temperature which indicates the values of M_r, and H_C.

Fig.5. shows the magnetic hysteresis loops for PANI/MFe_2O_4 nanocomposites at room temperature. Typical ferromagnetic loops are shown in Fig.5. (a, b). The magnetic parameters such as coercivity (H_C), saturation magnetization (M_S) and remanance magnetization (M_r) of the nanocomposites are given in Table 7. In the present study, the nanocomposites have lower M_s values compared with pure magnetic ferrite nanoparticles [22, 38]. This may be due to the existence of diamagnetic phase of PANI in the nanocomposites.

Table 7. Magnetic parameters of PANI/MFe_2O_4 nanocomposites such as saturation magnetization (M_S), coercivity (H_C), remanent magnetization (Mr) of nanocomposites.

Sample	Hc(Oe) PANI/MFe_2O_4	Ms(emu/g) PANI/MFe_2O_4	Ms(emu/g) MFe_2O_4 bulk sample	Mr(emu/g) PANI/MFe_2O_4
PANI/Fe_3O_4	79.33	64.23	84[a]	5.202
PANI/$CoFe_2O_4$	107.2	65.39	73[b]	8.138
PANI/$NiFe_2O_4$	68.48	≈ 0	55[c]	$6.657x10^{-3}$
PANI/$MnFe_2O_4$	76.98	≈ 0	110[d]	$5.959x10^{-3}$
PANI/$ZnFe_2O_4$	50.17	≈ 0	54[e]	0.07059

[a](Referenece [11]),[b](Referenece [14]), [c](Referenece [31]), [d](Referenece [32]), [e](Referenece [22]).

Fig.5. (a, b) together with Table 7 indicate that the PANI/Fe_3O_4 and PANI/$CoFe_2O_4$ are exhibited ferromagnetic behavior with small values of remanance magnetization (M_r). Sample of PANI/Fe_3O_4 nanocomposite showed a high-saturation magnetization of 64.23 emu/g in agreement with that recorded in literature [9, 11, and 39]. Moreover, Fig.5. (c-e) show the hysteresis loops of PANI/$NiFe_2O_4$, PANI/$MnFe_2O_4$, and PANI/$ZnFe_2O_4$ respectively, which have M_r and M_s values tends to zero. On the other hand the value of H_c does not decrease to zero (H_c=50-70 Oe). The reason may be attributed to the presence of few ferromagnetic clusters in the polymer matrix. The lack of rmanance M_r and saturation magnetization M_s indicated the presence of superparamagnetic particles, since the mean size of the ferrite nanoparticle is much close to the calculated critical size which is related to superparamagnetic behaviour [39-42].

It is worthy to note that the measured magnetization and the coercive force of nanocomposites are considerably lower than the values measured from bulk magnetic material (see Table 7), and the pure magnetic nanoparticles [22, 38, and 43]. Several reports described the decrease of M_s and H_c for the magnetic nanoparticles with nonmagnetic matrix (polymer). The observed magnetic properties for magnetic nanoparticles are due to a combination of many anisotropy mechanisms, such as magnetocrystalline anisotropy, surface anisotropy and interparticles interactions [19, 43]. Interaction of MFe_2O_4 nanoparticles with PANI may affect the contributions of the surface anisotropy and interparticles interactions to the net anisotropy. Hence, the value of the net anisotropy for PANI/MFe_2O_4 nanocomposites may decrease with the decrease of MFe_2O_4 nanoparticles content which is due to the reduction of surface anisotropy. On the basis of the above discussion, the decrease in coercivity and magnetization with the decrease of MFe_2O_4 nanoparticles content is expected. By

now, no definite explanation of this discrepancy exists. This variation in the values of saturation magnetization can be generally attributed to the varying size of ferrite nanoparticles in each sample. However, the interactions between the polymer matrix and ferrite nanoparticles may play an important role in attaining the magnetic nature of these nanocomposites. The interaction between ferrite nanoparticles and PANI leads to a significant decrease in the magnetic nature of the overall nanocomposites, owing to the diamagnetic nature of PANI. The specific morphology of PANI as well as the surface chemistry influences the surface interactions of the magnetic nanoparticles strongly. Therefore, the measured values of M_s are so different due to the different interactions at the interphases in these nanocomposites [11, 30]. Moreover, the magnetic properties varied with different substituted metal cations, this is due to the change of the net magnetic moment of crystal unit of ferrite nanoparticles .So it gives an easy way to tune the magnetic properties of ferrite particles by using different metal salts during reaction process.

4. CONCLUSION

PANI/MFe_2O_4 nanocomposites (M = Fe^{2+}, Co^{2+}, Ni^{2+}, Mn^{2+}, and Zn^{2+}) were synthesized by in situ precipitation method. The obtained samples were characterized and the main results are summarized as follows:

- The XRD pattern of PANI/MFe_2O_4 nanocomposites shows that the Fe_3O_4 , $CoFe_2O_4$, $NiFe_2O_4$,$MnFe_2O_4$ and $ZnFe_2O_4$ nanoparticles species in these nanocomposites are cubic spinel structure with lattice constant a = 8.32Å, 8.36Å, 8.42 Å, 8.49 Å, and 8.46 Å respectively they all have the size in range from 10 to13 nm.
- PANI can minimize the agglomeration of MFe_2O_4 nanoparticles, and MFe_2O_4 nanoparticles are embedded in polymer chain.
- SEM images show that the average size of MFe_2O_4 nanoparticles is in the range 17 to 30 nm and exhibit spherical morphology.
- The result of particle size analyzer (PSA) shows that the mean size of PANI/MFe_2O_4 nanocomposites is in the range from 24 to 37nm.
- The magnetic MFe_2O_4 nanoparticles can improve the thermal stability of the nanocomposite due to the interaction between MFe_2O_4 nanoparticle and PANI chain.

PANI/Fe_3O_4 and PANI/$CoFe_2O_4$ nanocomposites are exhibited ferromagnetic behavior. The saturation magnetization was found to reduce by the addition of Mn, Ni, and Zn ions instead of Fe^{2+} and Co^{2+}.

References

1. A.Lagashetty and A. Venkataraman, *Resonance*, (2005) 49-60.
2. M. D. Ventra, S. Evoy, J. R. Heflin, "Introduction to Nanoscale Science and Technology", Kluwer Academic Publishers, (2004).
3. S. Aoshima , F. R. Costa , L. J. Fetters , G. Heinrich , S. Kanaoka, A. Radulescu , D. Richter , M. Saphiannikova , U. Wagenknecht , "Advances in Polymer Science", Springer-Verlag Berlin Heidelberg, vol 210, (2008).

4. J. Jiang, L. Li, M. Zhu, *Reactive & Functional Polymers* 68 (2008) 57–62.
5. L. Li, J. Jiang, F. Xu, *Materials Letters* 61 (2007) 1091–1096.
6. R. Mathur, D. R. Sharma, S. R. Vadera, N. Kumar, *Acta mater*. 49 (2001) 181–187.
7. L. Li, H. Liu, Y. Wang, J. Jiang, F. Xu, *Journal of Colloid and Interface Science* 321 (2008) 265–271.
8. A.G. MacDiarmid, A.J. Epstein, *Synthetic Metals* 69 (1995) 86-92.
9. J.C. Aphesteguy, S.E. Jacobo, *Physica B* 354 (2004) 224–227.
10. A. B. Moghaddam, T. Nazari, *Int. J. Electrochem. Sci.*, 3(2008)768-776
11. A. S. Sarac*, M. Ates and B. Kilic, *Int. J. Electrochem. Sci.*, 3(2008)777-786.
12. S. E. Jacobo, J. C. Aphesteguy, R. L. Anton, N.N. Schegoleva, G.V. Kurlyandskaya, *European Polymer Journal* 43 (2007) 1333–1346.
13. M.Wan, J.Fan, , Polym. Sci. part A: Polym. Chem.36(1998)2749; See also Y.I. Kim, Don Kim, C. Lee, *Physica* B 337 (2003) 42–51.
14. Y. Qu, H. Yang, N. Yang, Y. Fan, H. Zhu, G. Zou, Materials Letters 60 (2006) 3548–3552.
15. M.P. Gonzalez-Sandoval, A.M. Beesley, M. M.-Yoshida, L. F.-Cobas, J.A. M.-Aquino, *Journal of Alloys and Compounds* 369 (2004) 190–194.
16. G.V. Kurlyandskaya, J. Cunanana, S.M. Bhagata, J.C. Aphesteguy, S.E. Jacobo, *Journal of Physics and Chemistry of Solids* 68 (2007) 1527–1532.
17. J. H. Kim, F. F. Fang, H. J. Choi, Y. Seo, *Materials Letters* 62 (2008) 2897–2899.
18. N. V. Blinova, J. Stejskal, M. Trchová, J. Prokeš, M. Omastová, *European Polymer Journal* 43 (2007) 2331–2341.
19. J. Jiang, L. Li, F. Xu, *Journal of Physics and Chemistry of Solids* 68 (2007) 1656–1662.
20. H. Guo, H. Zhu, H. Lin, J. Zhang, *Materials Letters* 62 (2008) 2196–2199.
21. W. Xue, K. Fang, H. Qiu, J. Li, W. Mao, *Synthetic Metals* 156 (2006) 506–509.
22. C. Hu, Z. Gao, X. Yang, *Journal of Magnetism and Magnetic Materials* 320 (2008) L70–L73.
23. J. Deng, X. Ding, W. Zhang, Y. Peng, J. Wang, X. Long, P. Li, A. Chan, *Polymer* 43 (2002) 2179-2184.
24. N. S. Ramgir, Y. K. Hwang, I. S. Mulla, J.-S. Chang, *Solid State Sciences* 8 (2006) 359–362.
25. V. D. Pokhodenko, V. A. Krylov, Y. I. Kurys, O. Y. Posudievsky, *Phys. Chem. Chem. Phys*., 1 (1999) 905-908.
26. S. Sathiyanarayanan, S. S. Azim, G. Venkatachari, *Synthetic Metals* 157 (2007) 751–757.
27. E.N. Konyushenko, N.E. Kazantseva , J. Stejskal, M. Trchová, J. Kovářová, I. Sapurina, M.M. Tomishko, O.V. Demicheva, J. Prokeš, *Journal of Magnetism and Magnetic Materials* 320 (2008) 231–240.
28. K. R. Reddy, K. P. Lee, A. I. Gopalan, Colloids and Surfaces A: Physicochem. *Eng. Aspects* 320 (2008) 49–56.
29. Ö. Yavuz, M. K. Ram, M. Aldissi, P. Poddar, S. Hariharan, *Journal of Materials Chemistry* 15 (2005) 810–817.
30. J. Alam, U. Riaz, S. Ahmad, *Journal of Magnetism and Magnetic Materials* 314 (2007) 93–99.
31. L. Bao, J.S. Jiang, Physica B 367 (2005) 182–187.
32. Z. Cao, W. Jiang, X. Ye, X. Gong, *Journal of Magnetism and Magnetic Materials* 320 (2008) 1499–1502.
33. C. Yu, J. Zhai, Z. Li, M. Wan, M. Gao, L. Jiang, *Thin Solid Films* (2008).
34. M. Kryszewski, J.K. Jeszka, *Synthetic Metals* 94 (1998) 99-104.
35. X. M. Liu, S. Y. Fu, H. M. Xiao, C. J. Huang, *Physica* B 370 (2005) 14–21.
36. A.F. Júnior, E. C. de Oliveira Lima, M. A. Novak, P. R. Wells Jr, *Journal of Magnetism and Magnetic Materials* 308 (2007) 198–202.
37. S.-P. Lee, Y.-J. Chen, C.-M. Ho, C.-P. Chang, Y.-S. Hong, *Materials Science and Engineering* B 143 (2007) 1–6.

38. G.-y. Li, Y.-r. Jiang, K.-l. Huang, P. Ding, J. Chen, *Journal of Alloys and Compounds* 466 (2008) 451–456.
39. J.Laska, J.Widlarz, *Polymer* 46(2005)1485.
40. W.H.Meiklejohn, Rev.*Modern Phys*, 25(1953)302.
41. S.Chikazumi, S.Taketomi, M.Ukila, M.Mizukami, H.Miyajima, M.Setogawa, J.*Magn. Magn. Mater*, 65(1987)245.
42. Kodama et.al., *Phys.Rev. Lett.* 77(1996)394.
43. Q. Xiao, X. Tan, L. Ji, J. Xue, *Synthetic Metals* 157 (2007) 784–791.